

FIG. 1.

FIG. 2.

used as a sensitive indicator of radioactive contamination in the air, i.e., for air monitoring. Further simplification (which also represents a considerable increase of efficiency) was obtained by directing the stream of air toward a nuclear plate and collecting dust together with radioactive atoms on the surface of the emulsion. By a suitable arrangement many air samples can be taken with the same stripe of the plate. Figure 1 shows a typical dust-spot on the surface of an Ilford C2 emulsion obtained by aspirating 125 cc of air containing  $1.5 \times 10^{-13}$  Curie/cc of radon and developed 4 hours after taking the sample. Figure 2 shows alpha-ray tracks on the same area of the plate after removal of the dust-spot. In this area some 280 tracks were counted which, assuming radioactive equilibrium in the air, would mean that nearly 20 percent of the atoms of active deposit were collected with the dust on the plate. This percentage may depend on the instrument used and/or on the dust-conditions in the air. The method seems capable of detecting quantities as low as  $10^{-13}$  Curie of active deposit of radon.

Experiments have also been arranged in order to detect radioactive atoms in free atmospheric air. On dust-spots obtained by aspirating 1600 cc of free atmospheric air, on an average, 35 alpha-tracks were found. Most of them could be identified as alpha-particles of RaC. Assuming 20 percent efficiency, this would correspond to a radon concentration of  $10^{-15}$  Curie/cc which is fairly consistent with the value found, for example, by G. Aliverti<sup>3</sup> by an ionometric method.

Using electron sensitive emulsions the method could be also applied for detection of artificial solid beta-emitters in the air. Low energy ends of electron tracks which would be most appropriate for counting could be found near the area of the dust-spot by energies up to 0.3 Mev.

The author would like to thank Dr. Běhounek for helpful discussions. A detailed account of the method with some applications will be published elsewhere.

<sup>1</sup> Č. Jech, Nature **163**, 570 (1949).

<sup>2</sup> F. Běhounek and E. Effenberger, Gerlands Beitr. z. Geophys. **59**, 74 (1942).

<sup>3</sup> G. Aliverti, Zeits. Geophysik **9**, 16 (1933).

### Neutron-Proton and Proton-Proton Cross Sections at 83 Mev

L. CASTILLEJO AND H. T. RICHARDSON  
University College, London, England

October 7, 1949

CAMAC and Bethe<sup>1</sup> have shown that with central forces only and a square-well potential it was possible to obtain the observed cross sections for  $n-p$  scattering at 80 Mev provided that the range was  $2.0 \times 10^{-13}$  cm. Later Blatt<sup>2</sup> showed that the triplet range must be reduced to about  $1.5 \times 10^{-13}$  cm to fit the experi-

mental values of coherent neutron scattering by crystals and by parahydrogen.

The following calculations have been performed, using square-well potentials, to test the possibility of obtaining the correct high energy scattering results by reducing the range of the central force in the triplet interaction. The tensor force has not been neglected but this involves increasing its range.

Two sets of force constants have been used:

	$r_0$	$r_c$	$r_t$	$V_0$	$V_c$	$V_t$
A.	2.8	1.6	3.08	11.9	39.3	10.04
B.	2.8	0	3.27	11.9	$v_1 = 4.49 \times 10^{11}$ cm <sup>-1</sup>	9.62

where  $r$  is the range of the force in units of  $10^{-13}$  cm,  $V$  is the depth of the well in Mev, and the subscripts 0,  $c$ ,  $t$  denote singlet, central force triplet, and tensor force triplet interaction, respectively.

The singlet constants were chosen to fit the data on  $p-p$  scattering and the zero energy  $n-p$  cross section. The triplet constants were chosen to fit the binding energy, the quadrupole moment and the magnetic moment of the deuteron. Constants A were taken from the calculations of D. Padfield.<sup>3</sup> These agree reasonably well with results of coherent scattering of neutrons by parahydrogen and by NaH crystals since they give a zero energy triplet scattering length  $a_1 = -0.533$  as compared with an experimental value of  $-0.51$  to  $-0.53$ .<sup>4</sup> B was considered as the limiting case of  $r_c \rightarrow 0$  with  $V_c = \{(I/r_c^2) \sum v_n r_c^n\} \hbar^2/M$ , where from requirements of continuity  $v_0 = \pi^2/4$ . The constants in this case were calculated by F. Ledsham.<sup>5</sup>

Neutron-proton cross sections have been calculated at 83 Mev for symmetric and charged meson theory type of interactions and also for the mixture suggested by R. Serber in which only the even states interact. All phase calculations were performed exactly though the ( ${}^3D_3 + {}^3G_3$ ) and higher coupled phases were neglected. The total cross sections and the ratios of scattering at  $90^\circ$  and  $180^\circ$  are given in Table I and the differential cross sections in Fig. 1.

It would seem from these results that with the symmetric or charged theories there is no possibility of fitting the high energy data (at least with a square-well potential) by decreasing the central range  $r_c$ . This is shown in Fig. 2 where the total cross sections are plotted against  $r_c/r_t$ .<sup>6</sup> Though the high energy data might possibly be fitted by a Serber interaction, this has the disadvantage of introducing a new postulate, the amount of mixing of the symmetric and charged theories to account for the high energy scattering. Even then the single triplet range of  $2.8 \times 10^{-13}$  cm gives better results at 83 Mev though it does not, of course, fit the coherent scattering data.

*Scattering of like particles.*—Using the potential A, calculations have also been carried out for the  $p-p$  scattering at the same energy. To allow for the Coulomb interaction in the calculation of the nuclear phases, the equations were solved inside the well neglecting this potential and these solutions were fitted to Coulomb

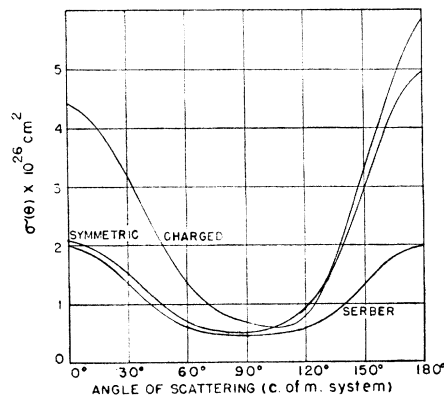


FIG. 1. Differential  $n-p$  cross section  $\sigma(\theta)$  for potential A.

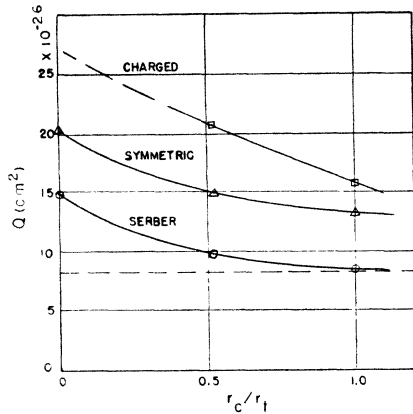


FIG. 2. Total cross section  $Q$  for symmetric, charged and Serber interactions plotted against  $r_c/r_t$ .

TABLE I. Total  $n-n$  and  $n-p$  cross sections  $Q$  in units of  $10^{-26} \text{ cm}^2$  and ratio of scattering at  $180^\circ$  to  $90^\circ$  for potentials  $A$  and  $B$ .

	A				B	
	Neutron-proton $Q$	$\frac{\sigma(180^\circ)}{\sigma(90^\circ)}$	Neutron-neutron $Q$	$\frac{\sigma(180^\circ)}{\sigma(90^\circ)}$	Neutron-proton $Q$	$\frac{\sigma(180^\circ)}{\sigma(90^\circ)}$
Symmetric	14.91	9.59	4.23	25.37	20.29	5.60
Charged	20.68	8.87	21.20	16.96	Over 22	—
Serber	9.92	4.09	—	—	14.92	4.64

wave functions as solutions outside the well. The phases were then corrected by adding a perturbation inside the well to allow for the Coulomb field there. The resulting phases differed in most cases by less than one percent from the  $n-p$  phases and the greatest difference was two percent. At this energy therefore it is reasonable to neglect the Coulomb potential in the calculation of the phases.

The angular distributions for  $n-n$  and  $p-p$  scattering are shown in Fig. 3 for the charged and symmetrical cases. The cross section at  $90^\circ$  (center-of-mass system) is considerably less than that given by Ashkin and Wu<sup>7</sup> at 100 Mev using the potential of Rarita and Schwinger<sup>8</sup> including the tensor forces. This could therefore be regarded as an effect arising from the double range.

At about  $15^\circ$  the  $p-p$  cross section falls below the  $n-n$ . The opposite is the case in the distributions described by Barker and Ravenhall<sup>9</sup> where the  $p-p$  cross section remains steadily above the

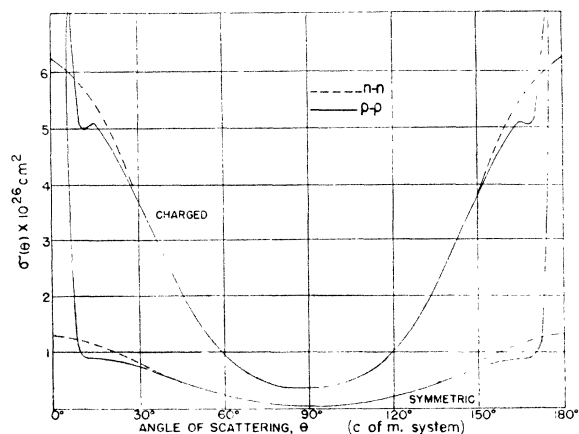


FIG. 3. Differential  $p-p$  and  $n-n$  cross sections for potential  $A$ .

$n-n$ . The reason for this is that in the central force case the  $^3P$  phase is negative and so the imaginary parts of the scattered amplitude add. For the potential used here, the  $^3P_0$  phase is large and positive, and the interference between the Coulomb and the nuclear wave gives rise to the above effect. The total cross sections for  $n-n$  scattering for the charged and symmetric cases and also the ratios of the differential cross sections at  $90^\circ$  to those at  $180^\circ$  are given in Table I.

We would like to thank Dr. Hu and Dr. Burhop for their assistance and suggestions, and Professor Massey for his continued interest.

- <sup>1</sup> M. Camac and H. A. Bethe, Phys. Rev. **73**, 191 (1948).
- <sup>2</sup> J. M. Blatt, Phys. Rev. **74**, 92 (1948).
- <sup>3</sup> D. Padfield, Nature **163**, 22 (1949).
- <sup>4</sup> R. B. Sutton *et al.*, Phys. Rev. **72**, 1147 (1947); C. G. Shull *et al.*, Phys. Rev. **73**, 842 (1948).
- <sup>5</sup> F. Ledsham (to be published).
- <sup>6</sup> Massey, Burhop, and Hu, Phys. Rev. **73**, 1403 (1948).
- <sup>7</sup> J. Ashkin and T. Wu, Phys. Rev. **73**, 973 (1948).
- <sup>8</sup> W. Rarita and J. Schwinger, Phys. Rev. **59**, 436 (1941); **59**, 556 (1941).
- <sup>9</sup> Barker and Ravenhall, Nature **163**, 20 (1949).

### Cosmic Rays at a Great Depth

Y. MIYAZAKI

Scientific Research Institute, Ltd., Tokyo, Japan  
September 30, 1949

AFTER our experiments<sup>1</sup> at 1400 meter water equivalent in Shimizu Tunnel by using arrangement I in Fig. 1, we continued the same kind of measurements at 3000 m.w.e. in the same tunnel from August, 1940, to the end of 1945 with the same apparatus, and proved that intensities at the latter point were about 1/10 those at the former depth as shown in Fig. 2. The intensity *versus* depth curve is given in Fig. 3. We also measured the absorption by lead of various thickness and found that the shape of the absorption curve was almost the same as at 1400-m.w.e. depth and the existence of showers was remarkable just as at 1400 m.w.e. Therefore the cosmic-ray particles at 1400- and 3000-m.w.e. depth are concluded to have the same nature. The absorption curve is of a form similar to that on the ground and therefore the particles are presumably mu-mesons which are the decay product of pi-mesons.

The showers-to-singles under various thicknesses of lead at the two depths can be seen from Fig. 2. They are about  $\frac{1}{4}$  and  $\frac{1}{3}$  at 1400 m.w.e. and 3000 m.w.e., respectively.

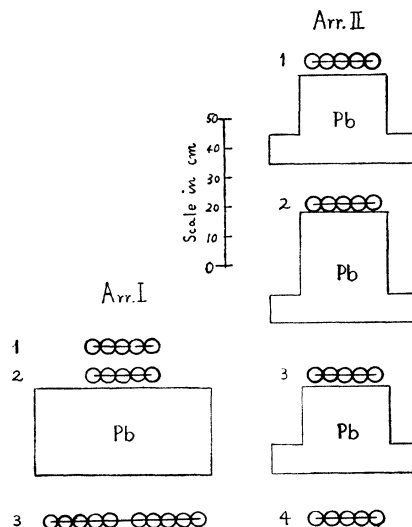


FIG. 1. Counter arrangement.